Attributing Tropical Cyclogenesis to Equatorial Waves in the Western North Pacific

CARL J. SCHRECK III

Cooperative Institute for Climate and Satellites, North Carolina State University, and the National Climatic Data Center, Asheville, North Carolina

JOHN MOLINARI

Department of Atmospheric and Environmental Sciences, University at Albany, State University of New York, Albany, New York

KAREN I. MOHR

Laboratory for Atmospheres, NASA Goddard Space Flight Center, Greenbelt, Maryland

(Manuscript received 2 December 2009, in final form 16 September 2010)

ABSTRACT

Tropical cyclogenesis is attributed to an equatorial wave when the filtered rainfall anomaly exceeds a threshold value at the genesis location. It is argued that 0 mm day^{-1} (simply requiring a positive anomaly) is too small a threshold because unrelated noise can produce a positive anomaly. A threshold of 6 mm day^{-1} is too large because two-thirds of storms would have no precursor disturbance. Between these extremes, consistent results are found for a range of thresholds from 2 to 4 mm day^{-1}.

Roughly twice as many tropical cyclones are attributed to tropical depression (TD)-type disturbances as to equatorial Rossby waves, mixed Rossby–gravity waves, or Kelvin waves. The influence of the Madden–Julian oscillation (MJO) is even smaller. The use of variables such as vorticity and vertical wind shear in other studies gives a larger contribution for the MJO. It is suggested that its direct influence on the rainfall in forming tropical cyclones is less than for other variables.

The impacts of tropical cyclone–related precipitation anomalies are also presented. Tropical cyclones can contribute more than 20% of the warm-season rainfall and 50% of its total variance. The influence of tropical cyclones on the equatorial wave spectrum is generally small. The exception occurs in shorter-wavelength westward-propagating waves, for which tropical cyclones represent up to 27% of the variance. Tropical cyclones also significantly contaminate wave-filtered rainfall anomalies in their immediate vicinity. To mitigate this effect, the tropical cyclone–related anomalies were removed before filtering in this study.

1. Introduction

Convectively coupled equatorial waves represent a significant portion of tropical convective variability (Kiladis et al. 2009). These waves include equatorial Rossby (ER) waves, mixed Rossby–gravity (MRG) waves, and Kelvin waves. The Madden–Julian oscillation (MJO; Zhang 2005) is another prominent source of convective variability that consists of convectively forced equatorial waves, but it does not follow any equatorial wave dispersion relation. Tropical depression (TD)-type disturbances are wavelike systems that are sometimes called easterly waves. In the western North Pacific, TD-type disturbances propagate westward with periods of 3–9 days and wavelengths of 2500–4000 km (Reed and Recker 1971; Lau and Lau 1990; Takayabu and Nitta 1993; Dunkerton and Baldwin 1995; Chang et al. 1996). For brevity, all of these features will be referred to as equatorial waves because they reside in equatorial regions and share wavelike properties.

TD-type disturbances have been frequently associated with western North Pacific tropical cyclogenesis in synoptic studies. Ritchie and Holland (1999) examined the large-scale patterns associated with tropical cyclogenesis in the western North Pacific over 8 yr. Out of 199 storms, 47% developed within TD-type disturbances. The majority of these tropical cyclones formed when the disturbance entered the monsoon confluence

Corresponding author address: Carl J. Schreck III, Cooperative Institute for Climate and Satellites-NC, National Climatic Data Center, 151 Patton Ave., Asheville, NC 28801.
E-mail: carl.schreck@noaa.gov

DOI: 10.1175/2010JAS3396.1

region. Fu et al. (2007) similarly found that TD-type disturbances were associated with 53% of the 34 western North Pacific tropical cyclones during 2000 and 2001.

Other equatorial wave types can also influence tropical cyclogenesis. Dickinson and Molinari (2002) studied three tropical cyclones that formed as a packet of MRG waves transitioned to TD-type structures. Each storm developed on the northeastern edge of the Northern Hemispheric cyclonic anomalies where the idealized MRG wave favors convection. Similarly, four of the tropical cyclones examined by Fu et al. (2007) developed from TD-type disturbances that originated from MRG waves. Case studies (Molinari et al. 2007; Schreck and Molinari 2009) have shown that ER waves can also stimulate cyclogenesis by enhancing the background convection and low-level cyclonic vorticity.

Bessafi and Wheeler (2006) investigated the modulation of tropical cyclones by equatorial waves in the southern Indian Ocean. They defined six active phases for each wave based on the two leading principal components (PCs) of its filtered outgoing longwave radiation (OLR). A wave's influence on cyclogenesis was quantified by the number of storms that formed during each of its phases. The MJO, ER waves, and Kelvin waves each produced significant basinwide modulations of cyclogenesis. For these waves, at least twice as many storms developed during the most favorable phase compared with the least favorable phase.

In the western North Pacific and Indian Oceans, Liebmann et al. (1994) found that twice as many tropical cyclones developed in association with negative (convective) MJO-filtered OLR anomalies as with positive anomalies. Similarly, Frank and Roundy (2006) observed that tropical cyclones were significantly more likely to form in association with negative wave-filtered OLR anomalies than with positive anomalies. Depending on the basin and equatorial wave type, 55%–85% of tropical cyclones formed in association with negative wave-filtered OLR anomalies.

Frank and Roundy (2006) also examined the relationship between tropical cyclogenesis and basinwide wave activity. A wave was considered active when the running mean of its basinwide variance exceeded a threshold. In the western North Pacific, tropical cyclones were as likely to form when this threshold was met as when it was not. Nonetheless, composites for storms that formed when a given wave was active showed wave-enhanced convection and low-level cyclonic vorticity at the genesis locations.

Tropical cyclones themselves produce large local anomalies that significantly contribute to the mean and variance for a variety of meteorological fields. For Pacific islands near 125°E, tropical cyclones generate 24%–62% of the July–October rainfall (Hsu et al. 2008; Kubota and Wang 2009). The highest percentages occur near Taiwan, while tropical cyclones tend to have a smaller influence on rainfall at lower latitudes (Rodgers et al. 2000; Kubota and Wang 2009).

Tropical cyclone–related anomalies can also project onto the filter bands typically used to identify equatorial waves. For example, they contribute more than half of the intraseasonal (20–80 day) variance of vorticity in some portions of the western North Pacific (Hsu et al. 2008). Frank and Roundy (2006) estimated the basinwide OLR variance produced by tropical cyclones in each equatorial wave band. They included these estimates in their variance thresholds to determine when each wave type was active. In other studies of equatorial waves, however, the effects of tropical cyclones on wave diagnostics have been ignored.

Section 3 demonstrates a method proposed by A. Aiyyer (2007, personal communication) for identifying and removing the tropical cyclone–related anomalies in unfiltered data. This approach reduces the rainfall associated with each storm toward its climatological mean using a weighting function. Removing the storm-related rainfall before filtering is advantageous because some storms affect the filtered fields more than others. Whereas Frank and Roundy (2006) used the same correction for all tropical cyclones, the approach in this paper removes the individual precipitation anomalies associated with each tropical cyclone. In this way, the combined influences of multiple storms can be accounted for, which was not possible with Frank and Roundy's method. Aiyyer's method will also be used to estimate the contamination of the overall equatorial wave spectrum by tropical cyclones.

Previously, the influences of equatorial waves on tropical cyclogenesis have been examined in three ways: individual case studies (Dickinson and Molinari 2002; Molinari et al. 2007; Schreck and Molinari 2009), composites of storms that developed while each wave was active (Frank and Roundy 2006), or counting the number of tropical cyclones that formed during each phase of the waves (Liebmann et al. 1994; Bessafi and Wheeler 2006; Frank and Roundy 2006). The current study takes a storm-centric approach by examining each tropical cyclone formation to determine which ones can be directly attributed to equatorial wave–enhanced convection. The results for each equatorial wave type will be tallied over many (145) storms to determine their relative importance for cyclogenesis. This approach will also identify storms that develop in association with multiple wave types, which previous climatologies have not examined.

Definition of attribution

A relatively narrow definition of attribution is used in this paper. Tropical cyclogenesis will be attributed to an equatorial wave when the filtered rainfall anomaly in the 1° grid box containing the genesis location exceeds a threshold value. This approach does not account for the dynamical or indirect influences of equatorial waves on cyclogenesis. While these are potentially significant omissions, the enhancement of convection is one of the primary mechanisms for equatorial waves to foster cyclogenesis (Dickinson and Molinari 2002; Liebmann et al. 1994; Frank and Roundy 2006).

To tie the attributions to the magnitude of convective enhancement, we apply the same threshold to all wave types and all genesis locations. Alternatively, each equatorial wave's threshold could be based on that wave's distribution of rainfall anomalies. Some wave types, on average, produce larger filtered anomalies than others do. However, equatorial waves that produce larger filtered rainfall anomalies are likely to exert a greater influence on convection and subsequently on cyclogenesis. This influence requires the same threshold for all wave types.

The wave-filtered rainfall anomalies only account for a small fraction of the total latent heating that occurs within a developing tropical cyclone. The role of the wave is to supply an environment within which deep convection and ultimately tropical cyclogenesis can occur (Liebmann et al. 1994; Briegel and Frank 1997; Dunkerton et al. 2008). Because of the difference in scale between the wave and the tropical cyclone, it is impossible to determine a single threshold objectively from basic principles. Instead, the attribution estimates will be calculated for a range of reasonable thresholds. It will be shown that the relative importance of the various wave types will be largely insensitive to the choice of thresholds within this range.

2. Data and analysis methods

Tropical cyclone tracks are obtained from the National Climate Data Center's (NCDC's) International Best Track Archive for Climate Stewardship (IBTrACS; Knapp et al. 2009). This dataset merges tropical cyclone data from operational centers around the world. Tropical cyclogenesis in the present study will be defined as the first time a storm achieves maximum 10-min sustained winds of at least 13 m s^{-1} (25 kt). The current study will focus on cyclogenesis in the western North Pacific during the warm seasons (May–November) from 1998 to 2007. The domain encompasses the region from the equator to 20°N and 120°E to the date line. Poleward of 20°N is excluded because tropical cyclogenesis in those regions is more likely to be associated with tropical transition (Davis and Bosart 2001) and upper-level troughs (Sadler 1976) than with equatorial waves. The domain also excludes the South China Sea westward of 120°E where land–ocean contrasts can influence convection and cyclogenesis.

The equatorial waves will be identified using the Tropical Rainfall Measuring Mission (TRMM) Multisatellite Precipitation Analysis (TMPA; TRMM product 3B42; Huffman et al. 2007). This dataset merges precipitation estimates from passive microwave sensors on a suite of low earth-orbiting satellites. Gaps between low earth-orbiting passes are filled using geostationary infrared data. The resulting precipitation estimates are then calibrated using global analyses of monthly rain gauge data. The TMPA data are available from 1998 onward on 3-hourly 0.25° latitude–longitude grids, but they have been averaged to 6-hourly 1° latitude–longitude grids to improve computational efficiency. The original 0.25° data contained a limited number of missing values comprising less than 6% of the entire dataset. The lack of geostationary infrared coverage over the Indian Ocean before June 1998 caused most of these gaps (Huffman et al. 2007). While averaging to the coarser grid, these missing data were interpolated bilinearly in space and linearly in time from the surrounding values. The waves investigated in this research are sufficiently broad in scale that the results will be insensitive to the averaging and interpolation.

Previous studies (e.g., Cho et al. 2004; Masunaga et al. 2006) have demonstrated the utility of similar datasets for analyzing equatorial waves. The rainfall data are advantageous because of their physical link to the diabatic heating required for tropical cyclone formation. The spatial and temporal resolution of this dataset also allows for better analysis of the environment for tropical cyclogenesis, which might be difficult to resolve with 2.5° daily OLR data.

Figure 1 shows the wavenumber–frequency power spectrum for the TMPA rainfall rates calculated following Wheeler and Kiladis (1999). To focus on warm season signals, the spectra are computed for overlapping 96-day segments that begin 30 March, 1 May, 2 June, 4 July, 5 August, and 6 September in each year 1998–2007. The segments extend beyond May–November to account for the tapering that is applied to each segment. These spectra are also calculated at each latitude from the equator to 15°N with no equatorial symmetry constraints. The variance is then averaged from all of these latitudes and time segments, and Fig. 1a shows the base-10 logarithm of this mean spectrum.

Figure 1 is qualitatively similar to analogous spectra of OLR (Wheeler and Kiladis 1999; Roundy and Frank

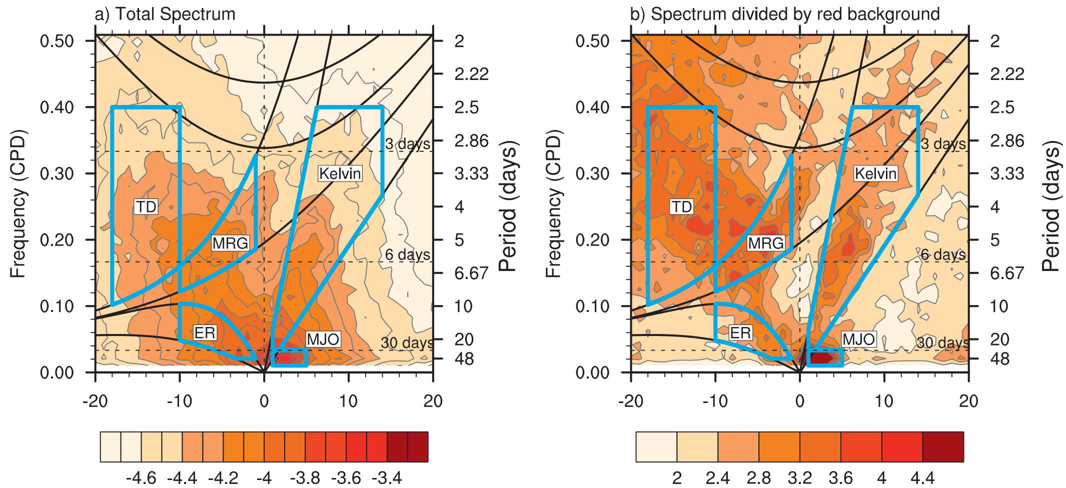

FIG. 1. (a) Total wavenumber–frequency power spectrum for warm season precipitation from the equator to 15°N. The base-10 logarithm of the power has been plotted. (b) As in (a), but normalized by a red background as in Roundy and Frank (2004). Filter bands are indicated by the cyan boxes. Black lines denote shallow-water dispersion curves for MRG, Kelvin, ER, and inertio-gravity waves with equivalent depths of 8 and 90 m.

2004). Some equatorial wave signals stand out even in the total spectrum (Fig. 1a). The most notable spectral peaks are associated with the MJO, Kelvin waves, and, to a lesser degree, MRG and ER waves. These features show more clearly in Fig. 1b where the spectrum is divided by a red background following Roundy and Frank (2004).

The cyan boxes in Fig. 1 define the filter bands used to identify the equatorial waves in this study. These bands, other than the TD band, are identical to those defined by Wheeler and Kiladis (1999). The TD band is defined as wavenumbers from −18 to −10 (2200–4000 km) and periods longer than 2.5 days but shorter than the MRG wave solution for an equivalent depth of 90 m (roughly 8 days). This range of wavelengths and periods is chosen to encompass previously observed characteristics of TD-type disturbances in the western Pacific (e.g., Dunkerton and Baldwin 1995; Chang et al. 1996). Kiladis et al. (2006) defined a somewhat different filter band for TD-type disturbances over West Africa. Their filter has been applied to TD-type disturbances in the Pacific Ocean (Serra et al. 2008), but it overlaps with the MRG band. The TD band filter in Fig. 1 should distinguish TD-type disturbances from MRG waves. This filter may also be more appropriate for the western North Pacific where TD-type disturbances exhibit longer periods than in other regions (Lau and Lau 1990; Chang et al. 1996).

3. Tropical cyclone–related anomalies

One possible method for investigating the influence of equatorial waves on tropical cyclogenesis is to composite many genesis events and look for evidence of the waves. Fig. 2a presents a time–longitude composite of all western North Pacific cyclone formations during the 1998–2007 warm seasons. The shading shows the composite rainfall rates centered on the genesis time and location, which are then filtered for each equatorial wave (only the +1 mm day^{-1} contours are shown).

The most prominent feature in Fig. 2a is the tropical cyclone itself, which appears as a westward-moving precipitation maximum. Even though this is a composite for genesis, the precipitation maximum dissipates with time. This dissipation is probably due to the tendency for tropical cyclones to move poleward away from the latitude at which they developed.

In addition to this sharp precipitation maximum, the unfiltered data in Fig. 2a indicate broad envelopes of weaker precipitation (8–16 mm day^{-1}) moving eastward and westward. The eastward-moving envelope coincides with the MJO anomalies (cyan contour), while the westward-moving envelopes roughly correspond with positive ER wave and TD-type anomalies (orange and dark red contours, respectively). The unfiltered rainfall rates associated with these features are less than 16 mm day^{-1}, which is much less than the 89 mm day^{-1} at the genesis location.

The large precipitation maximum associated with the composite tropical cyclone can project onto many filter bands, as illustrated in Fig. 2b. Here the precipitation field (shading) is defined to be a stationary maximum with the same magnitude (89 mm day^{-1}) as the composite tropical cyclone. The resulting filtered anomalies are contoured for each equatorial wave band at the same contour level as in Fig. 2a. This stationary maximum

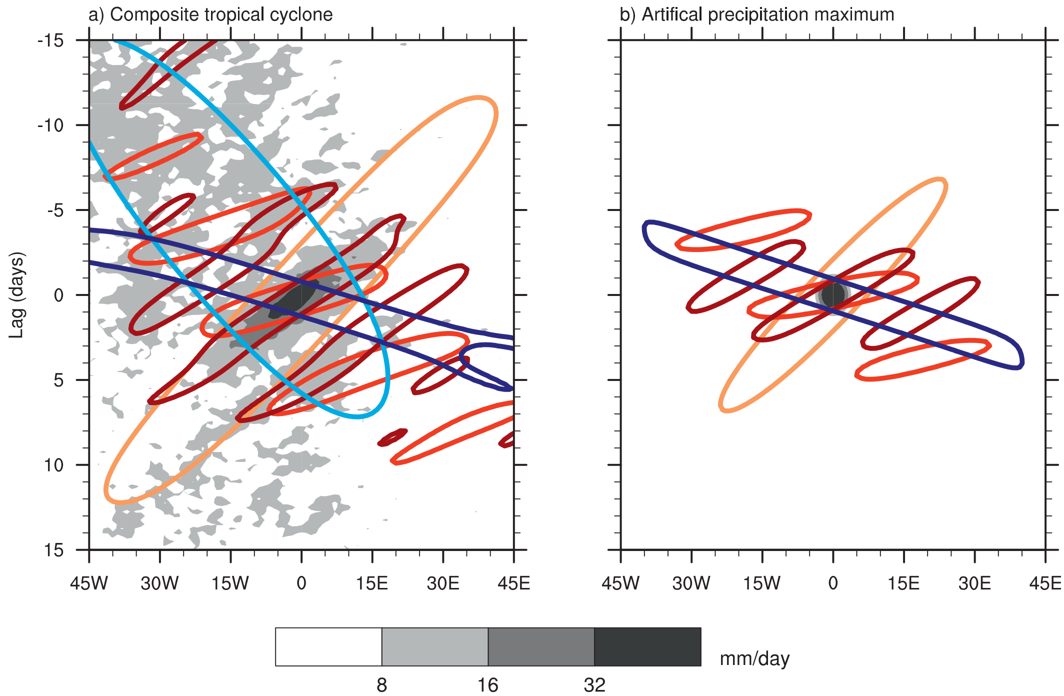

FIG. 2. (a) Time–longitude composite of western North Pacific tropical cyclogenesis. (b) Time–longitude plot of a prescribed stationary precipitation maximum. Shading indicates unfiltered fields, while filtered anomalies are contoured only at +1 mm day^{-1} for the MJO (cyan), Kelvin (blue), ER (orange), MRG (red), and TD bands (dark red).

should be completely unrelated to any propagating equatorial wave, yet it still projects strongly onto all of the filter bands except for the MJO. The artificial anomalies are generally weaker than those associated with the real composite, but the patterns are conspicuously similar. In addition to the positive anomalies centered on the stationary maximum, the filters also produce ringing with positive anomalies in regions where the unfiltered field is zero (e.g., the positive MRG anomalies centered at $\pm$4 days and $\pm$20° longitude).

Figure 2 demonstrates a significant obstacle to determining the influence of equatorial waves on tropical cyclones: It can be difficult to determine from filtered data which features are associated with equatorial waves and which are associated with the tropical cyclones themselves. The core dynamics of tropical cyclones produce large amounts of rainfall that are essentially unrelated to the dynamics of equatorial waves. Nonetheless, this intense rainfall projects onto the filtered fields.

Figure 3 uses an example from 0000 UTC 21 August 2000 to illustrate a method for isolating the tropical cyclone–related signals. At this time, a tropical depression that will later become Tropical Storm Kaemi has recently formed in the South China Sea. Meanwhile, Typhoon Billis lies to the east of the Philippines. Figure 3a shows a latitudinal cross section of rainfall through the center of Billis. The storm is associated with intense rainfall of 261 mm day^{-1} (red line). This rainfall rate is in the 99.9th percentile of the warm season precipitation data in the western Pacific (not shown). By contrast, the climatological rainfall rates (black line) are generally less than 10 mm day^{-1}. Because the data are only available for 10 yr, the climatology has been calculated by summing the first four harmonics of the annual cycle at each grid box. This procedure minimizes the impact of individual events on the climatology.

A. Aiyyer (2007, personal communication) proposed removing the tropical cyclone–related signals using a weighting function centered on each storm position. Here, we use a Gaussian function (dashed line in Fig. 3a):

$$w(x, y) = 1 - \exp\left\{-\frac{r(x, y)^2}{2[R(2\ln 2)^{-1/2}]^2}\right\}, \tag{1}$$

where $r(x, y)$ is the distance from a given grid point to the tropical cyclone's center and R is the radius at half maximum of the weighting function. To remove the tropical cyclone, the difference between the actual rainfall and its climatological value at each location is multiplied by the weight from Eq. (1). At zero radius of the tropical cyclone, all of the rainfall above climatology is removed, and the removal fraction decreases with radius following the Gaussian function in Eq. (1).

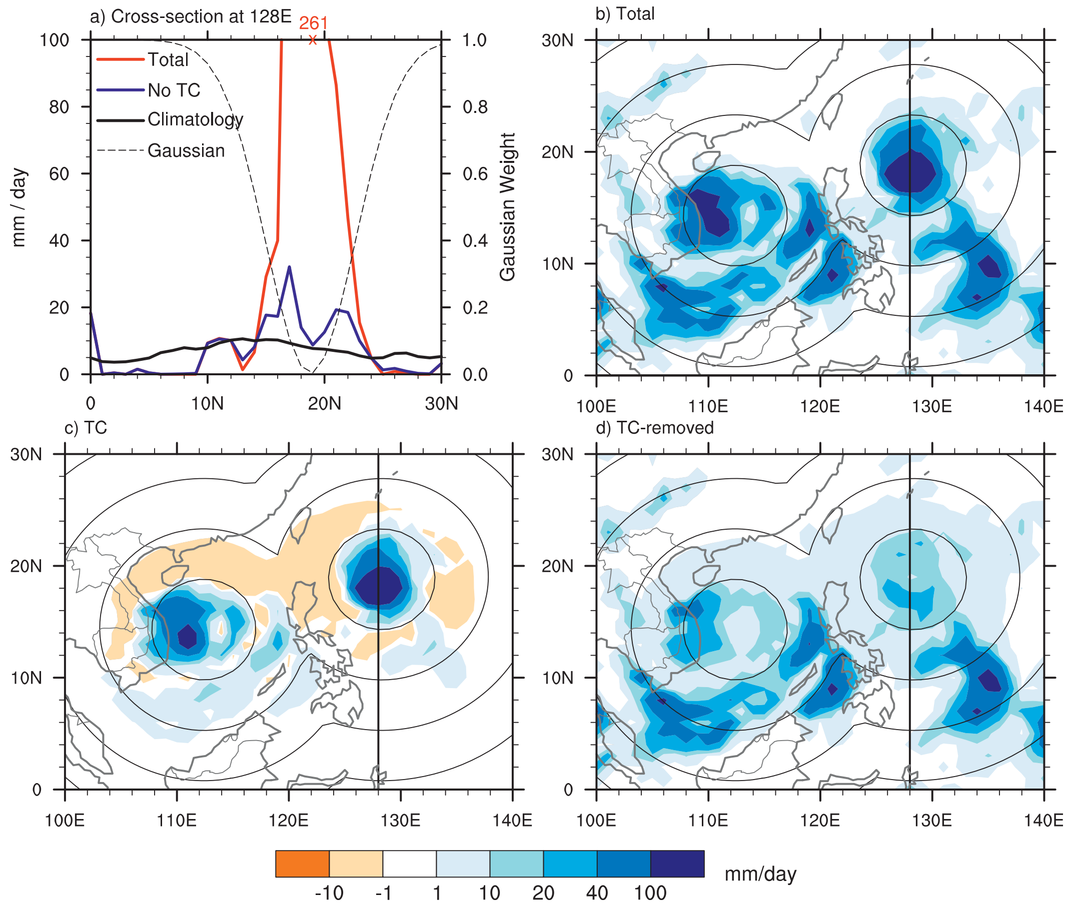

FIG. 3. Rainfall rates at 0000 UTC 21 Aug 2000. (a) Latitudinal section along 128°E of total rainfall (red), with tropical cyclones removed (blue), climatology (black), and the tropical cyclone weighting function. Maps of (b) total rainfall, (c) TC-related anomalies, and (d) modified rainfall rates following the TC removal. Black rings indicate the distance to the nearest TC every 500 km.

The blue line in Fig. 3a shows the resulting rainfall rate following the tropical cyclone removal. The rate of 261 mm day^{-1} in Billis's core is reduced to the climatological value of 8 mm day^{-1}. Anomalies at large distances (e.g., >1500 km) from the storm are virtually unchanged because they are completely attributed to the larger-scale environment (including equatorial waves). Using Eq. (1), anomalies at a distance R from the tropical cyclone are half associated with the storm and half associated with the environment. We use R = 500 km, but the results presented in this study are not sensitive to the details of the removal (see the appendix). Equation (1) is applied in all basins and to all tropical cyclone positions (not just genesis) that meet the minimum intensity of 13 m s^{-1}. Removing the anomalies associated with all tropical cyclones is important because Fig. 2 demonstrates that a storm can contaminate filtered fields at large distances in space and time.

Figure 3b shows a map of the total precipitation, while the anomalies attributed to tropical cyclones are shown in Fig. 3c. The weighting is applied to positive and negative rainfall anomalies alike. The core dynamics of the tropical cyclones generate the positive anomalies associated with the storm, but tropical cyclones also create negative anomalies nearby through compensating subsidence. This subsidence manifests itself as the moat of negative rainfall anomalies surrounding each storm's core.

Figure 3d displays the modified precipitation field with the tropical cyclones removed. The tropical cyclone–related anomalies (Fig. 3c) are subtracted from the original data (Fig. 3b) to produce this modified rainfall. The precipitation in the cores of the tropical cyclones (within 500 km) has been greatly reduced, while the shield of light rainfall (<10 mm day^{-1}) has been expanded around the storms. Some remaining features, such as the cyclonically curved band of rainfall to the north of Borneo, might or might not be attributable to the tropical cyclones. Nevertheless, the appendix shows that doubling R in Eq. (1) to 1000 km has a negligible impact on the results of this paper.

Figures 4a and 5a show the warm season mean and variance, respectively, of the original precipitation data.

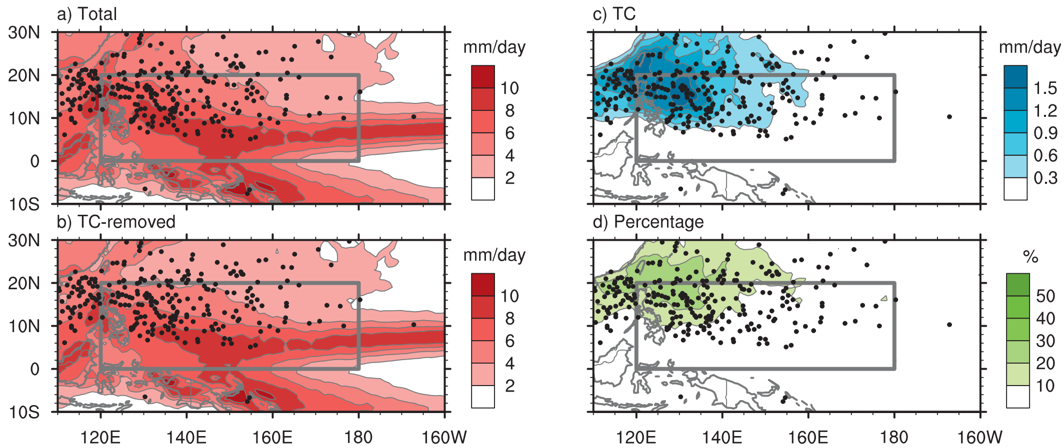

FIG. 4. Mean rainfall rate (mm day^{-1}) during May–November 1998–2007: (a) total rainfall, (b) rainfall with the TCs removed, (c) TC-related rainfall, and (d) TC contribution (%). Black dots indicate cyclogenesis locations for the same period.

Both fields are largest in a band that extends northwestward from the intertropical convergence zone (ITCZ) in the central Pacific. The striking similarity between the patterns of the mean and variance is typical for convective precipitation, which is highly variable by nature. This convection provides a preferred region for cyclogenesis although the storms (black dots) generally develop on the northern side of the convective maximum.

The general pattern of the precipitation mean and variance remains similar following the removal of the tropical cyclone signals (Figs. 4b and 5b). The most prominent difference is the weakened rainfall variance to the east of the Philippines. The ITCZ still dominates, but the tropical cyclones apparently extended the convective maximum to the northwest (cf. Figs. 4a,b and 5a,b).

The mean and variance of the tropical cyclone–related rainfall anomalies are shown in Figs. 4c and 5c, respectively. The tropical cyclones contribute strongly to the mean and variance of rainfall in the northwestern portion of the basin where the concentration of storms is greatest. In this region, the tropical cyclones are responsible for more than 20% of the mean rainfall and 50% of its variance (Figs. 4d and 5d).

As illustrated by Fig. 2, the intense rainfall associated with tropical cyclones can contaminate the filtered fields that are frequently used to identify equatorial waves. Figure 6a quantifies the contamination by showing the difference between the original spectrum (Fig. 1a) and the spectrum following the tropical cyclone removal (not shown). At first glance, Fig. 6a suggests a serious concern for previous climatologies of equatorial waves (e.g., Wheeler and Kiladis 1999): tropical cyclones produce power in nearly all of the equatorial wave filter bands. However, the contours in Fig. 6a, which represent the base-10 logarithm of the variance, are smaller than in Fig. 1a. To illustrate the difference in magnitude, Fig. 6b

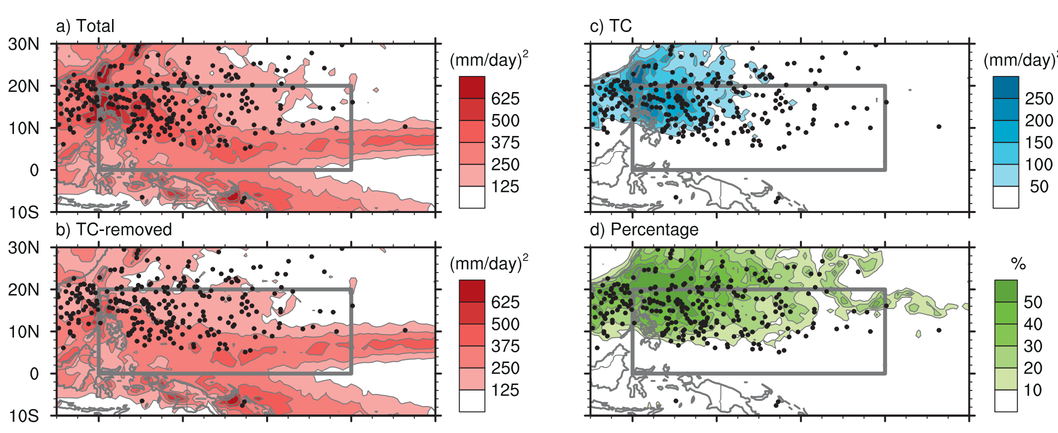

FIG. 5. As in Fig. 4, but for rainfall variance [(mm day^{-1})^2].

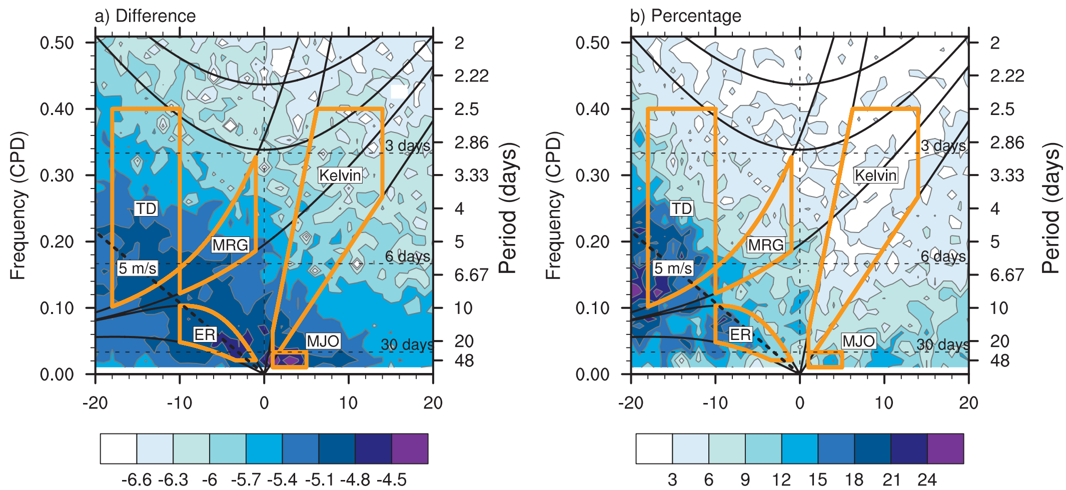

FIG. 6. (a) Difference between the total spectra of the original data and the TC-removed data. (b) Percentage calculated by dividing (a) by the total spectrum of the original data.

shows the percentage of the total power (Fig. 1a) that is associated with tropical cyclone–related anomalies (Fig. 6a). The strongest tropical cyclone–related power falls within the MJO filter band (Fig. 6a), but the MJO power is much stronger in the total spectrum (Fig. 1a). Tropical cyclones contribute less than 15% of this peak (Fig. 6b).

In addition to the MJO peak, a portion of the tropical cyclone–related variance propagates westward at roughly 5 m s^{-1} (Fig. 6a, thick dashed line). Tropical cyclones generally move westward at low latitudes, so this signal may be expected. This variance falls within the ER filter band and the lower-frequency portions of the MRG and TD-type bands. Up to 27% of the total variance in these areas is associated with tropical cyclones (Fig. 6b). Figure 6 is calculated using a radius at half maximum of 500 km for the tropical cyclone–related anomalies. If this radius is doubled, the maximum tropical cyclone contribution to any portion of the spectrum is 34% (not shown).

For shorter wavelength ER waves, MRG waves, and TD-type disturbances, the contamination from tropical cyclone–related anomalies is large enough that these signals should be removed before calculating the rainfall spectrum. Figure 2 demonstrates an even larger influence on the filtered fields at genesis locations. This contamination must be addressed to examine the influences of equatorial waves on tropical cyclogenesis. The present study will mitigate these effects by using Eq. (1) to remove the anomalies associated with all tropical cyclones before filtering.

4. Attributing tropical cyclones to equatorial waves

Figure 7 uses the genesis of Typhoon Lingling at 0000 UTC 6 November 2001 to illustrate the attribution method. The shading in Fig. 7 depicts the unfiltered rainfall rates following the removal of the tropical cyclone–related anomalies. In this example, the precipitation data are then filtered for MRG waves, and the resulting MRG anomalies are contoured in red. The MRG filter produces an anomaly of 3.97 mm day^{-1} in the 1° grid box containing Lingling's genesis. This anomaly is positive, so the MRG wave appears to contribute favorably to genesis. It is unclear whether that anomaly is sufficient to attribute Lingling's formation to these waves. An attribution threshold must be selected against which this anomaly will be compared.

To aid this selection, Fig. 8 shows the percentage of all warm season western North Pacific data points that exceed a given threshold. Only 145 tropical cyclones

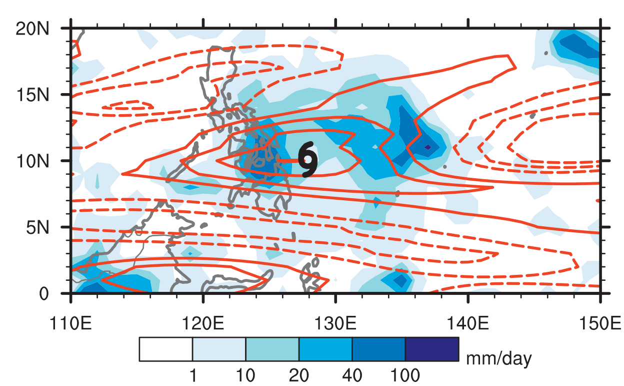

FIG. 7. Latitude–longitude section of unfiltered rainfall rates following TC removal (shading) and MRG-filtered rainfall anomalies (contours) at 0000 UTC 6 Nov 2001. Contours are drawn every 1 mm day^{-1} with the zero contour omitted and negative contours dashed. The hurricane symbol denotes the genesis location of Typhoon Lingling.

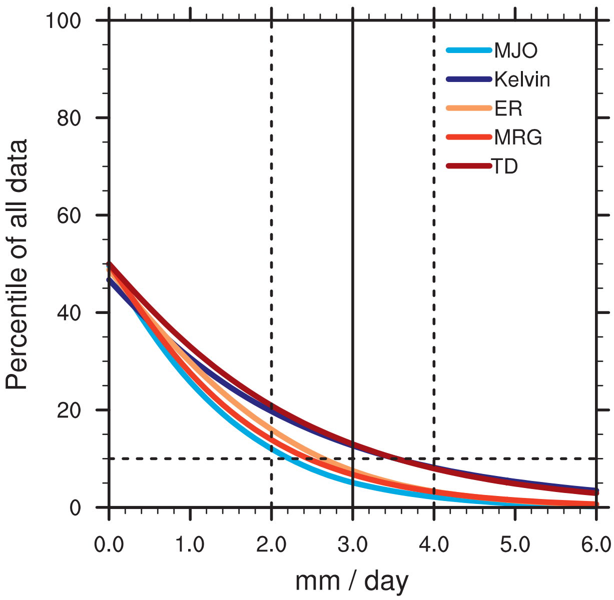

FIG. 8. Percentage of all warm season western Pacific data points that exceed a given threshold for the MJO (cyan), Kelvin waves (blue), ER waves (orange), MRG waves (red), or TD-type disturbances (dark red).

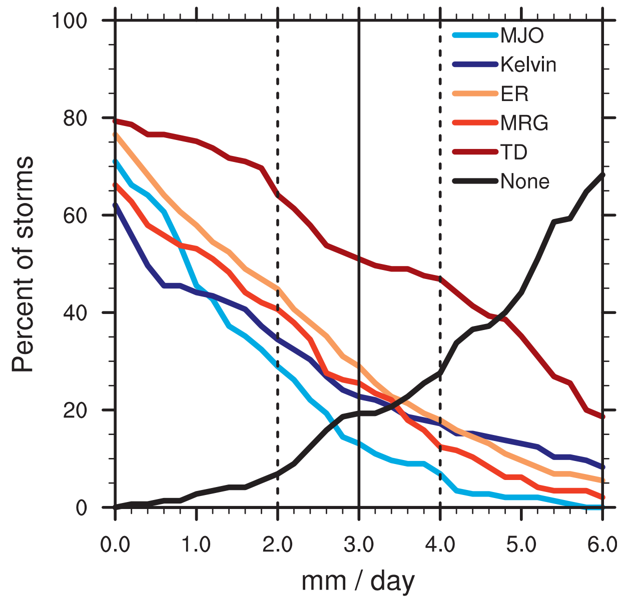

FIG. 9. Percentage of TCs that form associated with anomalies that exceed a given threshold for each filter band following TC removal using Eq. (1) with $R = 500$ km. Colors are as in Fig. 8, except the black curve indicates the percentage of storms for which none of the waves exceeds the threshold.

formed among the 2.6×10^6 total data points, so Fig. 8 essentially represents nongenesis points. The curves in this figure can also be thought of as the inverted cumulative density functions for each wave type. As expected with Fourier filtering, approximately one-half of the filtered data are positive. This fraction decreases for higher thresholds, and less than 4% of the data exceed 6 mm day^{-1}.

Figure 9 reveals the results of the attribution measures. It shows the percentage of the 145 warm season western North Pacific storms that developed while the filtered anomaly at the nearest grid point exceeded a given threshold. These percentages can sum to more than 100% because a given storm may be attributed to more than one wave. The black line indicates the percentage of storms for which none of the five equatorial wave types met the threshold. The percentage of genesis points exceeding a given threshold (Fig. 9) is almost always greater than the percentage of total points exceeding that same threshold (Fig. 8). Within the range of thresholds shown, the only exception is the MJO for thresholds greater than 5.8 mm day^{-1}. Even though Figs. 8 and 9 are calculated after removing the tropical cyclone–related signals, the genesis points are still associated with greater filtered rainfall anomalies than the nongenesis points.

Examining the attributions for each threshold in Fig. 9 provides some guidance for selecting the most appropriate threshold. For a zero threshold, which simply requires a positive filtered anomaly at the genesis location, 79% of the 145 tropical cyclones are attributed to TD-type disturbances (Fig. 9). The percentages are less for other equatorial waves, but each wave type generated positive anomalies for at least 62% of the storm formations. Even in the absence of wave activity, however, unrelated noise still produces positive anomalies for roughly 50% of the filtered data. It is unclear how many of the tropical cyclones that developed within positive TD-filtered anomalies were associated with actual TD-type disturbances. The zero threshold also fails to distinguish between wave types. Every tropical cyclone is attributed to at least one equatorial wave, and 16% of the storms are attributed to all five waves (not shown).

Anomalies of 6 mm day^{-1} represent only a small fraction of the 89 mm day^{-1} observed during tropical cyclogenesis (Fig. 2). However, the value of 6 mm day^{-1} surpasses the 95th percentile for each equatorial wave type (Fig. 8), and such an anomaly would almost certainly be associated with wave-enhanced convection. For this threshold, 68% of the storms have no equatorial wave precursor (Fig. 9). TD-type disturbances are associated with 19% of the tropical cyclone formations, and the percentages are even lower for the other waves. These results would contradict the link between wave precursors and cyclogenesis found by numerous previous studies (e.g., Riehl 1979, p. 465; Yanai 1961; Heta 1990; Fu et al. 2007).

TABLE 1. Number of TCs attributed to each wave type as a function of the number of contributing wave types. For example, the second row shows the number of storms associated with a single wave type, while the third row shows the number of storms attributed to each wave when two wave types met the threshold simultaneously. The rightmost column shows the total number of tropical cyclones attributed to zero, one, two, three, or four wave types. This column is not the sum of the others because a given storm may be counted under more than one column.

No. of wave types	TD type	MRG	ER	Kelvin	MJO	Total
0	—	—	—	—	—	28
1	27	5	5	10	2	49
2	32	19	23	14	12	50
3	13	11	13	7	4	16
4	2	2	1	2	1	2
Total	74	37	42	33	19	145

TABLE 2. Number of TCs attributed to each combination of two equatorial wave types. Storms attributed to three or more wave types are counted for each possible combination of two of those wave types. The table is symmetric about the diagonal.

	TD type	MRG	ER	Kelvin	MJO
TD type	—	24	21	11	8
MRG	24	—	14	5	4
ER	21	14	—	12	5
Kelvin	11	5	12	—	6
MJO	8	4	5	6	—

The arguments above suggest that 0 mm day^{-1} is too small a threshold and 6 mm day^{-1} is too large. In this paper a range of thresholds between 2 and 4 mm day^{-1} will be chosen. Figure 8 shows that these thresholds encompass the 90th percentile (horizontal dotted line) of the filtered data for each wave type and thus are likely to be associated with enhanced convection. In addition, they are small enough that less than one-third of the storms develop without a wave precursor.

For thresholds of 2–4 mm day^{-1}, 47%–64% of the tropical cyclones are attributed to TD-type disturbances, which is consistent with Ritchie and Holland (1999) and Fu et al. (2007). Tropical cyclogenesis is attributed to ER, MRG, and Kelvin waves only about half as often, while the MJO was even less influential. Given the sample size of 145 storms, the 90% confidence intervals for these percentages can be determined using the cumulative density function for a binomial distribution. These intervals are ±3%–7%, depending on the threshold and wave type. Based on these intervals, the percentages of storms attributed to ER waves, MRG waves, and Kelvin waves are not significantly different from each other. However, the significance tests confirm that TD-type disturbances are associated with the most tropical cyclones; the MJO is associated with the fewest.

The remaining results are similar for any threshold from 2 to 4 mm day^{-1}. For brevity, these results will only be shown for the 3 mm day^{-1} threshold, which lies in the middle of our range of acceptable values. Table 1 shows the number of tropical cyclones attributed to multiple equatorial wave types with the 3 mm day^{-1} threshold. Only 18 of the 145 storms are attributed to three or more equatorial waves. Unlike the zero threshold, no storms are attributed to all five wave types. Because more than two-thirds (99 of 145) of the storms are attributed to only one or two wave types, these attributions seem to meaningfully distinguish between the wave types.

Table 2 shows how many tropical cyclones are attributed to each combination of two equatorial wave types using the 3 mm day^{-1} threshold. The few storms that have three or four equatorial wave precursors are counted under each combination of two of those wave types. For example, a storm attributed to ER waves, MRG waves, and TD-type disturbances would be counted as ER–MRG, ER–TD, and MRG–TD.

Approximately one-half (74 of 145) of all western North Pacific tropical cyclones are attributed to TD-type disturbances with the 3 mm day^{-1} threshold (Table 1). Just by chance, we might expect that about one-half of the storms attributed to any other equatorial wave would also be attributed to TD-type disturbances. Table 2 shows that this is indeed the case for ER waves (21 of 42) and the MJO (8 of 19). Only one-third (11 of 33) of the storms attributed to Kelvin waves are also attributed to TD-type disturbances. These two wave types produce the largest filtered anomalies (Fig. 8), so they might have been expected to interact more frequently to favor cyclogenesis. However, Kelvin waves and TD-type disturbances move in opposite directions with relatively short periods (generally 2.5–9 days; Fig. 1). It is possible that their positive rainfall anomalies do not coincide for long enough to support cyclogenesis jointly.

Nearly two-thirds (24 of 37) of the storms attributed to MRG waves are also attributed to TD-type disturbances. Both wave types move westward with similar periods. This large fraction could indicate that the filters do not separate the two wave types adequately. If this is the case, then the same disturbance could appear simultaneously in both filters. The overlap could be physically meaningful, however. Dickinson and Molinari (2002) showed that tropical cyclogenesis could occur when MRG waves transitioned to TD-type structures. These transitioning systems could explain the relatively large fraction of storms attributed to both wave types.

Figures 10a–e show the genesis locations of the storms attributed to each equatorial wave with the 3 mm day^{-1} threshold. These locations are overlaid on the warm season variance of the filtered precipitation for each

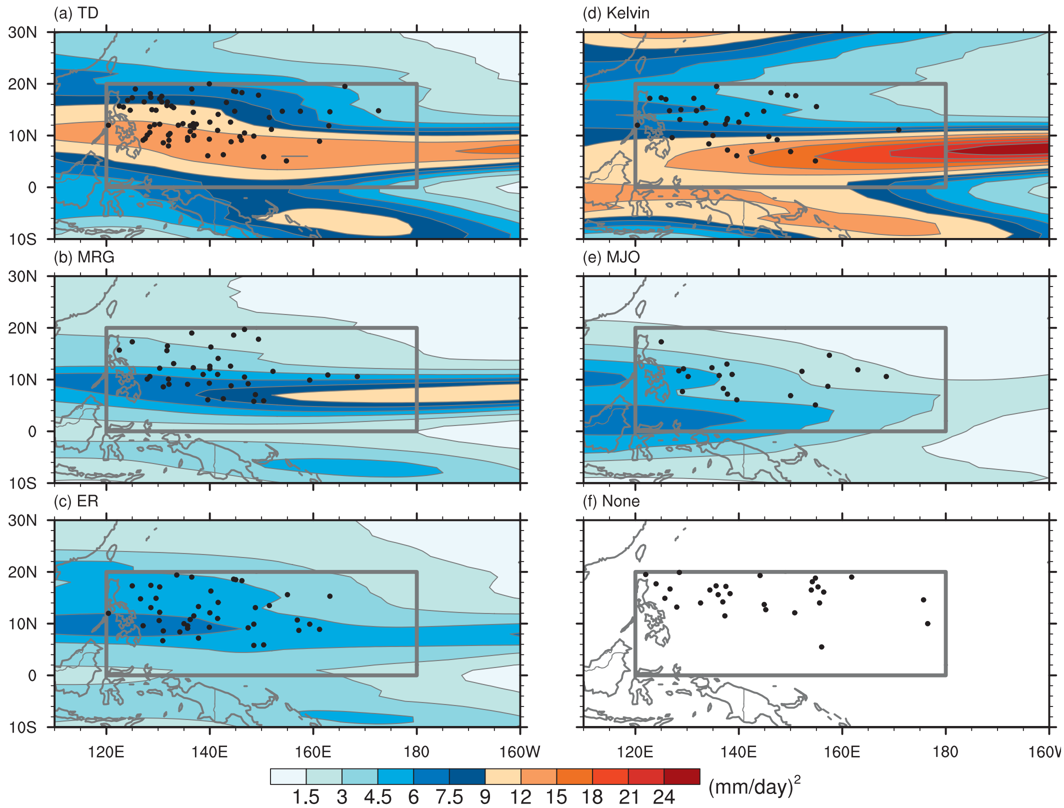

FIG. 10. Genesis locations for TCs attributed to (a) TD-type disturbances, (b) MRG waves, (c) ER waves, (d) Kelvin waves, and (e) the MJO overlaid on the warm season variance for the given filter band. (f) Genesis locations for TCs that were not attributed to any equatorial wave.

wave type, which are qualitatively similar to those found by Roundy and Frank (2004). The primary difference is that the variance maxima generally do not extend as far poleward in Fig. 10 because of the removal of the tropical cyclone–related anomalies.

The pattern of TD-type variance (Fig. 10a) resembles that of the total variance with the tropical cyclones removed (Fig. 5b), which is consistent with previous studies that have noted the prominence of TD-type disturbances in the western North Pacific (e.g., Reed and Recker 1971). By contrast, the MRG variance peaks in the central North Pacific (Fig. 10b). These patterns support previous studies that have shown MRG waves transitioning to TD-type structures in the western North Pacific (Sobel and Bretherton 1999; Dickinson and Molinari 2002; Aiyyer and Molinari 2003; Fu et al. 2007). The MJO variance (Fig. 10e) is concentrated in the western North Pacific, while the Kelvin wave variance (Fig. 10d) is stronger in the central North Pacific ITCZ. Consistent with this pattern, previous studies (e.g., Hendon and Salby 1994; Straub and Kiladis 2003) have observed Kelvin waves radiating to the east of the MJO as it dissipates.

The tropical cyclones attributed to MRG waves typically formed farther equatorward than other storms. The mean genesis latitude for all western North Pacific tropical cyclones from the equator to 20°N is 13.4°N while the mean for the MRG-related storms is 11.8°N. This difference is significant at the 95% level using either a Student's t test or a bootstrap test. Similarly, the mean latitude for storms attributed to the MJO is 10.4°N, which is also significantly equatorward of the overall mean.

Figure 10f shows the genesis locations of storms for which none of the equatorial waves met the 3 mm day^{-1} threshold. Only one tropical cyclone developed equatorward of 10°N without an equatorial wave precursor, and the mean genesis latitude for these storms is 15.4°N. This mean latitude is significantly farther north than that for all western North Pacific tropical cyclones. Not surprisingly, these results indicate that equatorial waves are most likely to affect cyclogenesis close to the equator.

5. Discussion and conclusions

This study identified tropical cyclones that developed in association with the equatorial wave–enhanced convection.

The results are used to examine the relative number of tropical cyclones that can be attributed to each equatorial wave type. Storms that form in association with multiple waves are also identified. In addition, tropical cyclones themselves contribute significantly to the convective variability in the western North Pacific (Fig. 5), and tropical cyclone–related variance can contaminate equatorial wave–filtered fields. This study isolates and removes the unfiltered tropical cyclone–related rainfall anomalies to quantify and mitigate this effect.

a. Tropical cyclone signals

The heavy precipitation associated with tropical cyclones accounts for more than 20% of the total warm season mean rainfall in some portions the western North Pacific (Fig. 4d). Tropical cyclones can also contribute 50% of the rainfall variance (Fig. 5d). Consistent with previous studies (e.g., Rodgers et al. 2000; Kubota and Wang 2009), tropical cyclones exert their greatest influence on rainfall near Taiwan and to the east of the Philippines (Figs. 4 and 5). The tropical cyclone–related rainfall also occurs poleward of the largest nontropical cyclone rainfall. Rodgers et al. (2000) found a similar pattern with the maximum tropical cyclone–related rainfall 5°–10° latitude poleward of the maximum total rainfall. Tropical cyclones seem to play an important role in extending the convection poleward from the ITCZ.

Much of the tropical cyclone–related rainfall variance falls within the equatorial wave filter bands (Fig. 6a). Tropical cyclones produce their largest spectral peak within the MJO band, but this signal represents less than 15% of the total MJO peak (Fig. 6b). If the MJO were simply a manifestation of tropical cyclones, then this percentage would be much larger. More likely, the MJO peak in Fig. 6a arises from the modulation of the tropical cyclones by the MJO itself. Tropical cyclones contribute a greater percentage of the total variance at the shorter wavelengths of the ER, MRG, and TD-type bands. Low-latitude storms frequently move westward at speeds that are similar to these waves, and the resulting contamination can be as much as 27% of the total signal.

The percentages in Fig. 6b are small enough that tropical cyclone signals probably did not overly affect previous climatologies of equatorial waves (e.g., Wheeler and Kiladis 1999; Yang et al. 2003; Roundy and Frank 2004). At the same time, they should be acknowledged in future studies, particularly those that use rainfall data. The largest spurious signals occur in the immediate vicinity of the tropical cyclones (Fig. 2), so they can distort the relationship between equatorial waves and tropical cyclogenesis. The current study mitigates this contamination by removing the tropical cyclone–related signals before filtering.

b. Equatorial wave attributions

Tropical cyclogenesis was attributed to an equatorial wave if the filtered anomaly exceeded a threshold value in the 1° latitude–longitude box containing the genesis location. The percentage of storms attributed to each wave type is sensitive to the threshold selection, but the relative importance of each wave type is consistent for a range of thresholds from 2 to 4 mm day^{-1}. These thresholds are strict enough to ensure convective enhancement but also lenient enough that at least two-thirds of the tropical cyclones have a wave precursor. TD-type disturbances are associated with the most tropical cyclones, regardless of the threshold. For thresholds from 2 to 4 mm day^{-1}, roughly twice as many tropical cyclones are attributed to TD-type disturbances as to ER waves, MRG waves, or Kelvin waves. Fewer tropical cyclones are attributed to the MJO than to any other wave type.

One-fifth of the tropical cyclones were not attributed to any equatorial wave using the 3 mm day^{-1} threshold. In the absence of an equatorial wave precursor, these storms could have been the product of upper-level trough interactions (Sadler 1976), tropical transition (Davis and Bosart 2001), or localized mesoscale convective systems within the monsoon trough (Ritchie and Holland 1999). The storms with no equatorial wave precursor typically originated farther poleward than other storms (Fig. 10f). Upper-level troughs and tropical transition are more common at higher latitudes, which would be consistent with this pattern.

Figure 9 shows that the MJO contributes less rainfall at genesis locations than other wave types, which have smaller spatial and temporal scales. However, past studies (e.g., Liebmann et al. 1994; Bessafi and Wheeler 2006; Kim et al. 2008) have shown that the MJO can significantly modulate tropical cyclogenesis. The MJO is a planetary-scale feature that produces large envelopes of favorable conditions. Tropical cyclogenesis may respond more to the MJO's modulation of other fields than to convection. For example, the MJO is known to influence cyclogenesis by modulating low-level vorticity (Hall et al. 2001), low-level convergence (Liebmann et al. 1994), vertical wind shear (Maloney and Hartmann 2000), and midlevel relative humidity (Camargo et al. 2009). The MJO also affects cyclogenesis by modulating the amplitudes of higher-frequency waves (Nakazawa 1988; Aiyyer and Molinari 2003). None of these influences was included in the rainfall attributions in this study. Future studies should develop attribution criteria that incorporate additional dynamical and thermodynamical factors. In addition, the attributions should be extended to other basins to quantify the importance of equatorial waves for cyclogenesis in those regions.

The results of this and future attribution studies should be relevant to forecasters. Equatorial waves can be identified and forecasted in real time with statistical methods (Wheeler and Weickmann 2001; Roundy and Schreck 2009). Such forecasts could be combined with the attribution information in Fig. 9 to indicate where and when an equatorial wave might favor cyclogenesis. This approach would be complementary to current regression models that forecast cyclogenesis based on equatorial waves (Frank and Roundy 2006; Leroy and Wheeler 2008).

Acknowledgments. This research has benefited greatly from conversations with Anantha Aiyyer, Paul Roundy, and Adam Sobel. We also thank the three anonymous reviewers whose insightful comments significantly improved this paper. We obtained the TMPA data from the NASA Goddard Distributed Active Archive Center (online at http://disc.sci.gsfc.nasa.gov/data/datapool/TRMM/). We are grateful to Dave Vollaro for his assistance in obtaining and interpolating this data. This work was supported by NSF Grant ATM0839991 and NASA Precipitation Measuring Mission Grant NNX07AD45G.

APPENDIX

Sensitivity of Attributions to the Method of Tropical Cyclone Removal

In this study, the anomalies associated with every tropical cyclone were removed. This procedure uses a Gaussian function [Eq. (1)] centered on the storm to separate the anomalies associated with the storm from those associated with the larger-scale environment (including equatorial waves). Anomalies at a radius $R = 500$ km were considered half associated with each. The remaining data were then filtered to determine which tropical cyclone formations were influenced by equatorial waves.

Figure A1 shows the sensitivity of the attributions to the method of tropical cyclone removal. Each panel is similar to Fig. 9, except for a different removal method. Fig. A1a uses the original rainfall data with no tropical cyclone removal. The results of doubling the radius at half maximum (R) for the Gaussian method [Eq. (1)] are shown in Fig. A1b. The Gaussian removal is somewhat arbitrary, so Fig. A1c presents the attribution results for removing the tropical cyclones with bilinear interpolation. In this case, a circle with a 500-km radius is identified around each tropical cyclone. All data points within that circle are bilinearly interpolated in space from the data on the perimeter.

The overall patterns in Fig. A1 are remarkably similar to those in Fig. 9. In each case, TD-type disturbances are associated with the most tropical cyclones, while the MJO

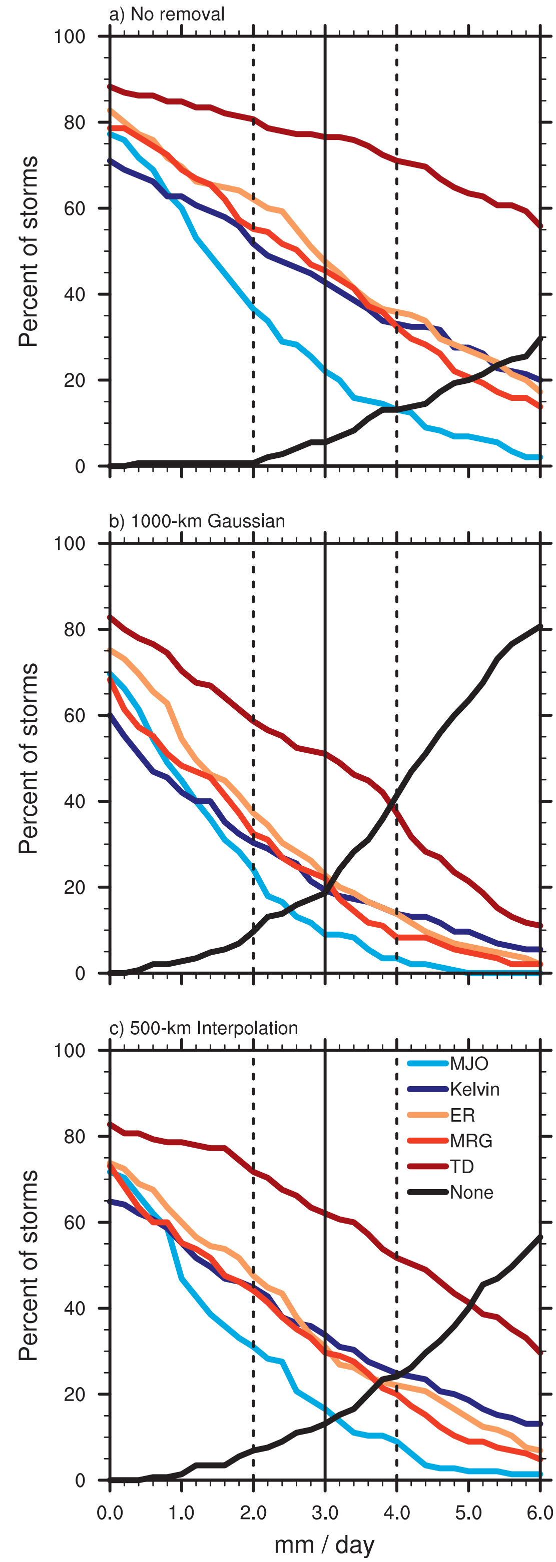

FIG. A1. As in Fig. 9, but for (a) no TC removal, (b) TC removal using Eq. (1) with $R = 1000$ km, and (c) TC removal by bilinearly interpolating over a circle with a 500-km radius centered on each storm.

is generally associated with the fewest. The percentages of storms attributed to ER waves, MRG waves, and Kelvin waves are comparable to each other and generally fall between those for TD-type disturbances and the MJO.

When the tropical cyclone signals are not removed, more storms are attributed to each wave type, particularly at higher thresholds. For the 3 mm day^{-1} threshold, removing the tropical cyclones decreases the percentage of storms attributed to TD-type disturbances from 76% (Fig. A1a) to 51% (Fig. 9). The contamination of the filtered fields by the tropical cyclones causes these differences.

Doubling the radius at half maximum of the removal from 500 to 1000 km has a minimal effect on the attributions (Fig. A1b). For the 3 mm day^{-1} threshold, the percentage of storms attributed to ER waves decreases from 29% (Fig. 9) to 23% (Fig. A1b), and the differences are even smaller for the other waves. Some tropical cyclone–related signals may be left behind by the removal for $R = 500$ km (Fig. 3d), but Fig. A1b suggests that these remaining signals have a negligible effect on the attribution results.

The percentages of storms attributed to each wave type are somewhat larger for the 500-km interpolation (Fig. A1c) than the 500-km Gaussian (Fig. 9). As with no removal, the differences are largest at higher thresholds. Kelvin waves and TD-type disturbances are also more sensitive to the removal method. Using the interpolation method, the percentages of tropical cyclones attributed to each of these wave types increases by 11%. In general, Fig. A1 shows that the attribution results are not overly sensitive to the details of the tropical cyclone removal.

REFERENCES

Aiyyer, A. R., and J. Molinari, 2003: Evolution of mixed Rossby–gravity waves in idealized MJO environments. *J. Atmos. Sci.,* **60,** 2837–2855.

Bessafi, M., and M. C. Wheeler, 2006: Modulation of South Indian Ocean tropical cyclones by the Madden–Julian oscillation and convectively coupled equatorial waves. *Mon. Wea. Rev.,* **134,** 638–656.

Briegel, L. M., and W. M. Frank, 1997: Large-scale influences on tropical cyclogenesis in the western North Pacific. *Mon. Wea. Rev.,* **125,** 1397–1413.

Camargo, S. J., M. C. Wheeler, and A. H. Sobel, 2009: Diagnosis of the MJO modulation of tropical cyclogenesis using an empirical index. *J. Atmos. Sci.,* **66,** 3061–3074.

Chang, C. P., J. M. Chen, P. A. Harr, and L. E. Carr, 1996: Northwestward-propagating wave patterns over the tropical western North Pacific during summer. *Mon. Wea. Rev.,* **124,** 2245–2266.

Cho, H.-K., K. P. Bowman, and G. R. North, 2004: Equatorial waves including the Madden–Julian oscillation in TRMM rainfall and OLR data. *J. Climate,* **17,** 4387–4406.

Davis, C. A., and L. F. Bosart, 2001: Numerical simulations of the genesis of Hurricane Diana (1984). Part I: Control simulation. *Mon. Wea. Rev.,* **129,** 1859–1881.

Dickinson, M., and J. Molinari, 2002: Mixed Rossby–gravity waves and western Pacific tropical cyclogenesis. Part I: Synoptic evolution. *J. Atmos. Sci.,* **59,** 2183–2196.

Dunkerton, T. J., and M. P. Baldwin, 1995: Observation of 3–6-day meridional wind oscillations over the tropical Pacific, 1973–1992: Horizontal structure and propagation. *J. Atmos. Sci.,* **52,** 1585–1601.

——, M. T. Montgomery, and Z. Wang, 2008: Tropical cyclogenesis in a tropical wave critical layer: Easterly waves. *Atmos. Chem. Phys. Discuss.,* **8,** 11 149–11 292.

Frank, W. M., and P. E. Roundy, 2006: The role of tropical waves in tropical cyclogenesis. *Mon. Wea. Rev.,* **134,** 2397–2417.

Fu, B., T. Li, M. S. Peng, and F. Weng, 2007: Analysis of tropical cyclogenesis in the western North Pacific for 2000 and 2001. *Wea. Forecasting,* **22,** 763–780.

Hall, J. D., A. J. Matthews, and D. J. Karoly, 2001: The modulation of tropical cyclone activity in the Australian region by the Madden–Julian oscillation. *Mon. Wea. Rev.,* **129,** 2970–2982.

Hendon, H. H., and M. L. Salby, 1994: The life cycle of the Madden–Julian oscillation. *J. Atmos. Sci.,* **51,** 2225–2237.

Heta, Y., 1990: An analysis of tropical wind fields in relation to typhoon formation over the western Pacific. *J. Meteor. Soc. Japan,* **68,** 65–77.

Hsu, H.-H., C.-H. Hung, A.-K. Lo, C.-C. Wu, and C.-W. Hung, 2008: Influence of tropical cyclones on the estimation of climate variability in the tropical western North Pacific. *J. Climate,* **21,** 2960–2975.

Huffman, G. J., and Coauthors, 2007: The TRMM Multisatellite Precipitation Analysis (TMPA): Quasi-global, multiyear, combined-sensor precipitation estimates at fine scales. *J. Hydrometeor.,* **8,** 38–55.

Kiladis, G. N., C. D. Thorncroft, and N. M. J. Hall, 2006: Three-dimensional structure and dynamics of African easterly waves. Part I: Observations. *J. Atmos. Sci.,* **63,** 2212–2230.

——, M. C. Wheeler, P. T. Haertel, K. H. Straub, and P. E. Roundy, 2009: Convectively coupled equatorial waves. *Rev. Geophys.,* **47,** RG2003, doi:10.1029/2008RG000266.

Kim, J.-H., C.-H. Ho, H.-S. Kim, C.-H. Sui, and S. K. Park, 2008: Systematic variation of summertime tropical cyclone activity in the western North Pacific in relation to the Madden–Julian oscillation. *J. Climate,* **21,** 1171–1191.

Knapp, K. R., M. C. Kruk, D. H. Levinson, and E. J. Gibney, 2009: Archive compiles new resource for global tropical cyclone research. *Eos, Trans. Amer. Geophys. Union,* **90,** 46, doi:10.1029/2009EO060002.

Kubota, H., and B. Wang, 2009: How much do tropical cyclones affect seasonal and interannual rainfall variability over the western North Pacific? *J. Climate,* **22,** 5495–5510.

Lau, K.-H., and N.-C. Lau, 1990: Observed structure and propagation characteristics of tropical summertime synoptic-scale disturbances. *Mon. Wea. Rev.,* **118,** 1888–1913.

Leroy, A., and M. C. Wheeler, 2008: Statistical prediction of weekly tropical cyclone activity in the Southern Hemisphere. *Mon. Wea. Rev.,* **136,** 3637–3654.

Liebmann, B., H. H. Hendon, and J. D. Glick, 1994: The relationship between tropical cyclones of the western Pacific and Indian Oceans and the Madden–Julian oscillation. *J. Meteor. Soc. Japan,* **72,** 401–412.

Maloney, E. D., and D. L. Hartmann, 2000: Modulation of eastern North Pacific hurricanes by the Madden–Julian oscillation. *J. Climate,* **13,** 1451–1460.

Masunaga, H., T. S. L'Ecuyer, and C. D. Kummerow, 2006: The Madden–Julian oscillation recorded in early observations from the Tropical Rainfall Measuring Mission (TRMM). *J. Atmos. Sci.,* **63,** 2777–2794.

Molinari, J., K. Lombardo, and D. Vollaro, 2007: Tropical cyclogenesis within an equatorial Rossby wave packet. *J. Atmos. Sci.,* **64,** 1301–1317.

Nakazawa, T., 1988: Tropical super clusters within intraseasonal variations over the western Pacific. *J. Meteor. Soc. Japan,* **66,** 823–839.

Reed, R. J., and E. E. Recker, 1971: Structure and properties of synoptic-scale wave disturbances in the equatorial western Pacific. *J. Atmos. Sci.,* **28,** 1117–1133.

Riehl, H., 1979: *Climate and Weather in the Tropics*. Academic Press, 611 pp.

Ritchie, E. A., and G. J. Holland, 1999: Large-scale patterns associated with tropical cyclogenesis in the western Pacific. *Mon. Wea. Rev.,* **127,** 2027–2043.

Rodgers, E. B., R. F. Adler, and H. F. Pierce, 2000: Contribution of tropical cyclones to the North Pacific climatological rainfall as observed from satellites. *J. Appl. Meteor.,* **39,** 1658–1678.

Roundy, P. E., and W. M. Frank, 2004: A climatology of waves in the equatorial region. *J. Atmos. Sci.,* **61,** 2105–2132.

——, and C. J. Schreck, 2009: A combined wavenumber–frequency and time-extended EOF approach for tracking the progress of modes of large-scale organized tropical convection. *Quart. J. Roy. Meteor. Soc.,* **135,** 161–173.

Sadler, J. C., 1976: A role of the tropical upper tropospheric trough in early season typhoon development. *Mon. Wea. Rev.,* **104,** 1266–1278.

Schreck, C. J., and J. Molinari, 2009: A case study of an outbreak of twin tropical cyclones. *Mon. Wea. Rev.,* **137,** 863–875.

Serra, Y. L., G. N. Kiladis, and M. F. Cronin, 2008: Horizontal and vertical structure of easterly waves in the Pacific ITCZ. *J. Atmos. Sci.,* **65,** 1266–1284.

Sobel, A. H., and C. S. Bretherton, 1999: Development of synoptic-scale disturbances over the summertime tropical northwest Pacific. *J. Atmos. Sci.,* **56,** 3106–3127.

Straub, K. H., and G. N. Kiladis, 2003: Extratropical forcing of convectively coupled Kelvin waves during austral winter. *J. Atmos. Sci.,* **60,** 526–543.

Takayabu, Y. N., and T. Nitta, 1993: 3-5 day-period disturbances coupled with convection over the tropical Pacific Ocean. *J. Meteor. Soc. Japan,* **71,** 221–246.

Wheeler, M., and G. N. Kiladis, 1999: Convectively coupled equatorial waves: Analysis of clouds and temperature in the wavenumber–frequency domain. *J. Atmos. Sci.,* **56,** 374–399.

——, and K. M. Weickmann, 2001: Real-time monitoring and prediction of modes of coherent synoptic to intraseasonal tropical variability. *Mon. Wea. Rev.,* **129,** 2677–2694.

Yanai, M., 1961: A detailed analysis of typhoon formation. *J. Meteor. Soc. Japan,* **39,** 187–214.

Yang, G. Y., B. Hoskins, and J. Slingo, 2003: Convectively coupled equatorial waves: A new methodology for identifying wave structures in observational data. *J. Atmos. Sci.,* **60,** 1637–1654.

Zhang, C., 2005: Madden-Julian oscillation. *Rev. Geophys.,* **43,** RG2003, doi:10.1029/2004RG000158.